LHC-CRI Technical Note 98-19
1999-03-04
(daniel.willems@cern.ch)

CTM3, THE LATEST EVOLUTION OF THE CRYOSTAT THERMAL MODEL: THERMAL PERFORMANCE MEASUREMENTS OF THE FIRST RUN FROM MARCH TO MAY 1998

Darve Ch., Poncet A., Willems D.

Abstract

A first measurement campaign of the latest of 3 series of Cryostat Thermal Models, CTM3, took place between March and May 1998. CTM3 features the near to final design of the LHC arc dipole cryostat with, in addition to the 50-75 K thermal shield, the option of a hard shield, actively cooled at 5-10 K, the radiation screen.

This note presents the preliminary performance of the cryostat, measured during this first campaign.

1. CTM3: Introduction

CTM3 features the latest developments of the LHC arc cryostat [1]. It has two levels of heat intercept. The thermal shield (50-75 K), made of a lengthwise segmented 2.5-mm thick aluminium shell welded on an extruded bottom tray, is covered with a multilayer insulation system (MLI) of type C [1] composed of 30 layers. The bottom tray, which incorporates the cooling line E (Figure 1.1), is welded onto the corresponding heat intercept of the cold mass support post, via a multilayer flexible aluminium strap.

The radiation screen, of a similar design, operates at 5-10 K, is covered with 10 layers of MLI of type C, and is separated from the 1.9 K cold mass by carbon-carbon composite spacers of high thermal impedance, with a functional thickness of 4 mm [2].

CTM3 presents improvements drawn from the experience of CTM2: All thermalisations and intercepts are welded (aluminium sheets on trays, aluminium straps from trays to support post intercepts, which have been sized to yield low temperature gradients with nominal heat loads).

The differences between CTM3 and the real LHC arc dipole cryostat and the differences between CTM3 and CTM2 are shown in Tables 1.1 and 1.2 respectively [3]. More details can be obtained at http://nicewww.cern.ch/~cdarve.

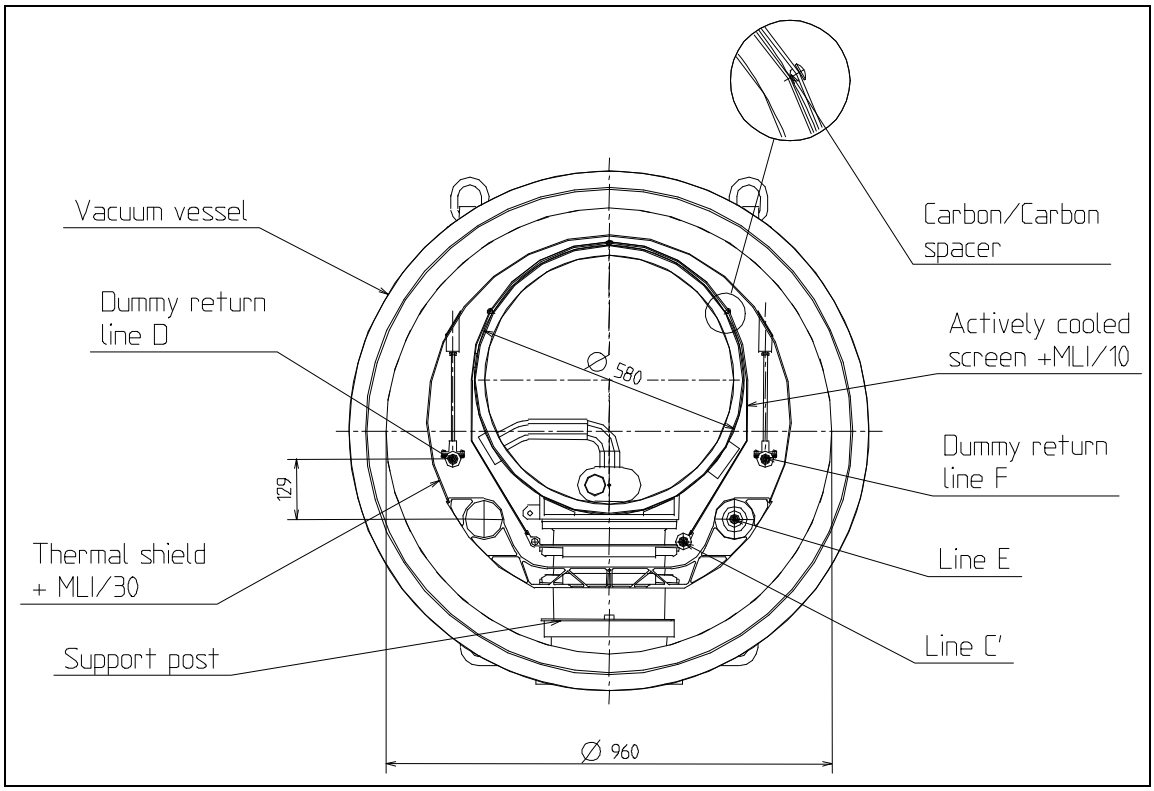

Figure 1.1: Design of CTM3

	LHC 15 m dipole cryostat	**CTM3**
Length of the vacuum vessel [mm]	14 560	9 852
Length of the cold mass [mm]	15 160	10 262
Inner diameter of the vacuum vessel [mm]	890	960
Outer diameter of the cold mass [mm]	570	580
Number of support posts	3	2
Distance between support posts [mm]	5 400	5 420

Table 1.1: Differences in dimensions between the 15-m LHC dipole cryostat and CTM3

	CTM2	CTM3
Thermal Shield	7 panels	
- inner diameter [mm]	884	806
- thickness [mm]	2.5	2.5
- bottom tray thickness [mm]	5	3 / 4 / 8
- assembly	Riveting	Welding on 20% of the length
Superinsulation	30 layers type C	30 layers type C
Thermalisation (Line E, F)	Screwed	Extrusion, welded 20% of the length
Radiation Screen	7 panels	
- inner diameter [mm]	810	580
- thickness [mm]	1.5	2.5
- assembly: bottom tray and upper shell	Riveting	Welding on 20% of the length
- bottom tray thickness [mm]	2	4
Superinsulation	10 layers type C	10 layers type C
Thermalisation (Line C)	braids/ copper 40 mm^2 * 115 mm	Extrusion and welding on 20% of the length

Table 1.2: Differences between CTM2 and CTM3

2. CTM3 run 1: Experimental campaign from March to May 1998

2.1 Foreword

Unlike previous CTM experimental campaigns, performed in SM18 equipped with a helium liquifier, CTM3-run1 used large helium dewars. This rendered the experiments difficult, because of the limited capacity of the dewars, related to the very long temperature stabilisation times due to very low thermal diffusivities of the MLI systems and the background pressure stabilisation.

It appeared early during the test campaign, that there were helium leaks into the insulation vacuum of CTM3. Upon reassembly during the autumn of 1998, it was found that welds had cracked in the dummy cold mass double wall envelope, and that a bellows was leaking.

2.2 Instrumentation and measurement methods

CTM3 incorporates a large number of temperature sensors at various levels, as shown schematically in Figure 2.1:

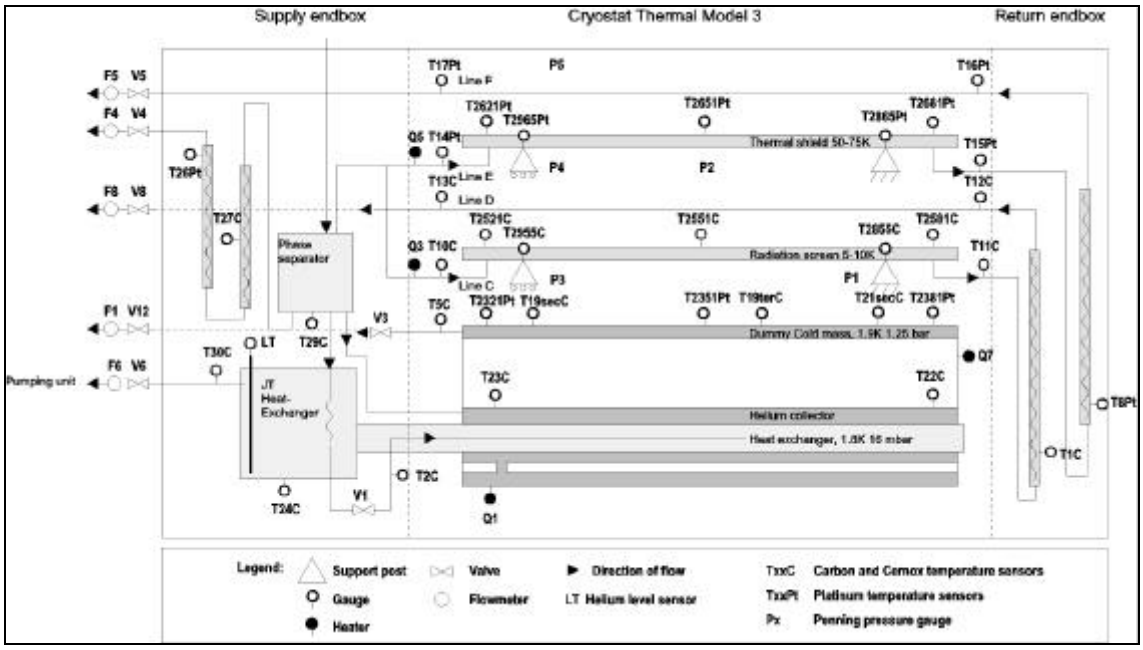

Figure 2.1: CTM3 sensor configuration

As for its predecessors, CTM3 heat loads at the various temperature stages are assessed from measurements of the extracted heat via the cooling circuits, obtained from differences in the enthalpy of the cooling gas, of known mass flow rates, between inlets and outlets, using equation 2.1 (applied to the thermal shield (50-70 K) and the radiation screen (5-10 K)):

$$\dot{Q} = \dot{m} \cdot [H(T_2) - H(T_1)] \qquad (2.1)$$

with H the enthalpy, T_2 and T_1 the helium temperatures at exit and entry, and $\dot{m}$ the mass flow rate. Electrical resistors of known values are used to cross check the calibration of the measurements. At 1.9 K, the heat load is obtained by measuring the helium boil-off rate from the static helium bath (eq. 2.2):

$$\dot{Q} = \dot{m} \cdot L_v \qquad (2.2)$$

with $\dot{m}$ the mass flow rate of the boiled off vapour, and L_v the latent heat of vaporisation at 1.9 K.

The expected precision of the measured heat loads to the different temperature levels are given in Table 2.1 [3]:

Temperature level:	Precision: [W]
Thermal shield (50 K-75 K)	+/-3
Radiation screen (5 K-10 K)	+/-0.15
Cold mass (1.9 K)	+/- 0.1

Table 2.1: Measurement precision in CTM3

Background gas density measurements are performed with Penning gauges, calibrated in pressure at room temperature. CTM3 uses 5 gauges, one on the vacuum vessel wall (300 K), two on the bottom tray of the thermal shield (50-75 K) and two on the bottom tray of the radiation screen (5-10 K).

2.3 Parasitic heat inleaks from feed and return boxes

During the CTM1 experimental campaign, the CTM feedbox, whose function is to provide gas flow and controls to the heat intercepts, the production of 1.9 K superfluid helium to the dummy cold mass and through which most of the instrumentation wires transit, had been partly reconfigured and equipped with commercially available helium control valves.

Although partly assessable and calculated from known values, the parasitic heat inleaks had not been measured prior to the first run of CTM3.

These measurements have been performed during the summer 1998, while CTM3 was being reconfigured for the second measurement campaign, and are reported in reference [9]. Table 2.2 below gives the parasitic heat inleak to the 1.9 K dummy cold mass as a function of residual helium pressure:

Insulating vacuum pressure P_{warm}, [mbar]	**Heat load to 1.9 K [mW]**
$1.27 \cdot 10^{-5}$	390
$1.11 \cdot 10^{-3}$	530
$3.9 \cdot 10^{-3}$	730

Table 2.2: Parasitic heat inleak from the feedbox

2.4 Thermal performance of the support post system

The support posts used to carry the 1.9 K dummy cold mass and the thermal shield are of the latest LHC design, for future use in the LHC dipole cryostat [6]. CTM3 does not provide the means to measure heat inleaks through the support posts directly. However, temperature sensors placed on the posts heat intercept flanges and on the screens bottom trays permit the thermal impedance of the welded aluminium straps linking the two to be verified, and thus check the quality of the thermalisation. These sensors also provide the necessary information to estimate indirectly the heat loads to shields and cold mass coming from the support posts, as measured in separate laboratory measurements [5].

Based on these measurements, a mathematical model describing the thermal behaviour has been established, which is used to estimate the loads coming from the posts over the complete measurement range of CTM3 [5], and allows an evaluation of the radiative and conduction performance of the shields alone.

2.5 Thermal performance of the cryogenic pin spacers

The thermal performance of the 42 pin spacers used to insulate the radiation screen from the cold mass has been measured at the central cryogenic laboratory (Cryolab). The results showed that for a cold mass of 1.86 K and a radiation screen temperature of 10 K with a pressure of 10^{-5} mbar, the heat load through the 42 spacers is about 2.9 mW. This is negligible compared to the total heat load. More results can be found in reference [2].

3. Experimental results

3.1 Nominal performance in good vacuum

The early occurrence of a helium leak from a ruptured weld in the cold mass rendered the experiments with good vacuum difficult. During most of the experimental campaign, the insulation vacuum had to be continuously pumped with a turbo molecular pump.

The simultaneous occurrence of the necessary conditions to obtain nominal and stable good vacuum conditions happened only a couple of times during the measurement campaign:

- 1.9 K and 4.5 K surfaces free from cryopumped helium.
- A full dewar at the beginning of the measurement.

The schematic in Figure 3.1 indicates the CTM3 temperature map, in an insulating vacuum pressure of $7 \cdot 10^{-7}$mbar (gauge reading on the vacuum vessel), and heat load values at the three temperature levels.

Temperature sensors placed on the support post intercepts, on the shields aluminium shells, and on the bottom trays for each temperature level show maximum differences of about 2 Kelvin. With the cooling gas flow rates used and indicated in the figure, the helium outlet temperatures of the two shields differ by less than one degree from those measured on the hard aluminium shields.

Table 3.1 below summarises the performance measured under good vacuum conditions. The net values are obtained from the total extracted heat measurements after subtraction of the support post and end box contributions (§ 2.3 and 2.4). They give an estimate of the thermal performance of the shields.

The heat load values quoted for the support posts have been obtained in a separate test cryostat [5]. The CTM3 mounting conditions being different from those in the test cryostat, in particular the thermal conductance of the bolted joints on the cold mass and the vacuum vessel, mean that the values obtained have to be considered with caution.

	Mass flow [g/s]		**Average temperatures [K]**			**Heat loads [W]**			
	Line E	**Line C**	**TS**	**RS**	**CM**	**Q_{TS}**	**Q_{RS}**	**Q_{CM}**	
P_{warm}:$7.5 \cdot 10^{-7}$ mbar						43.16	3.1	0.441	Total
								0.39	End boxes
						14.93	1.1	0.129	Support posts
Date: 22-May-'98	0.4	0.1	67.8	8.7	1.8	28.23	2.0	0	Net Values

Table 3.1: Results of CTM3 for nominal conditions

For reasons already given, the nominal vacuum conditions were never reproduced. Apart from the series of measurements under degraded vacuum conditions during which helium was deliberately injected, all other measurements were performed with a background pressure ranging from 10^{-6} to 10^{-5} mbar.

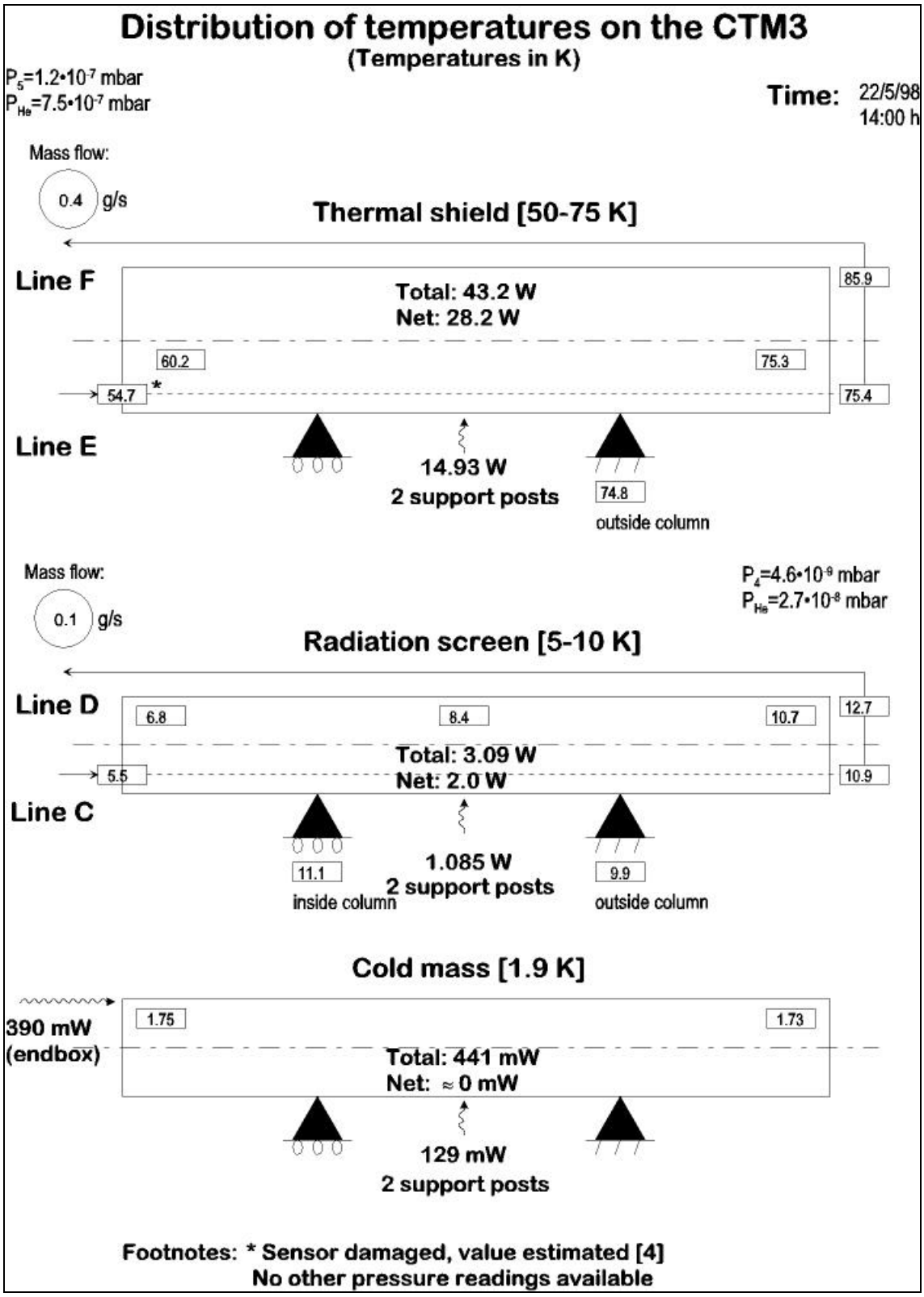

Figure 3.1: Temperature map and heat flow scheme of CTM3, nominal conditions

3.2 Measurements with radiation screen temperature degradation

To evaluate the performance of the actively cooled radiation screen, a series of measurements was performed with different temperatures of this screen.

The measurements were performed with approximately constant helium background pressure of $1.1 \cdot 10^{-5}$ mbar measured on the vacuum vessel, and of $1.6 \cdot 10^{-5}$ to $2 \cdot 10^{-5}$ mbar measured between cold mass and radiation screen. There were two series of measurements, with two different temperatures of the thermal shield. Using the appropriate heaters, the temperature of the gaseous helium at the entrance to line C was varied, along with the temperature of the radiation screen. The thermal performance of the support posts under these off design conditions was estimated using the mathematical model [5].

The results are given in table 3.2 and figure 3.3.

Temperatures [K]		Thermal shield [W]			Radiation screen [W]			Cold mass [W]		
T_{TS}	T_{RS}	Total	Supp.	Net	Total	Supp.	Net	Total	Supp.	Net
57	9.0	43.3	15.3	28.0	2.35	0.88	1.46	0.82	0.13	0.30
	11.6	40.8	15.3	25.4	1.77	0.80	0.97	1.05	0.17	0.50
	13.1	40.6	15.3	25.3	1.86	0.76	1.09	1.20	0.19	0.62
	15.0	41.7	15.4	26.4	1.61	0.69	0.92	1.30	0.23	0.68
	17.8	41.8	15.4	26.4	1.26	0.64	0.62	1.37	0.26	0.71
	20.3	42.9	15.4	27.5	1.05	0.57	0.48	1.55	0.31	0.86
	25.9	43.2	15.5	27.7	0.90	0.41	0.49	1.95	0.41	1.15
67	7.8	41.6	15.0	26.7	2.71	1.09	1.62	0.80	0.12	0.26
	16.0	43.3	15.0	28.4	2.34	0.89	1.45	1.03	0.24	0.40
	21.0	43.0	15.1	27.9	1.99	0.75	1.23	0.95	0.33	0.23

Table 3.2: Experimental results of CTM3 with degraded temperature of the radiation screen

The parasitic heat inleak via the end boxes to the cold mass is assumed constant at 390 mW over the range of off-design temperatures investigated. The net value for the heat inleak to the cold mass in the table is given by the total value, minus the endbox and support posts contributions.

3.3 Measurement without radiation screen cooling

One measurement was made without helium flow in the line C, thus disabling the active cooling of the radiation screen. Results for this measurement are shown in table 3.3 and the corresponding temperature map and heat flow scheme in figure 3.2.

	Mass flow [g/s]		Average temperatures [K]			Heat loads [W]			
	Line E	Line C	TS	RS	CM	Q_{TS}	Q_{RS}	Q_{CM}	
P_{warm}:$4.4 \cdot 10^{-6}$ mbar						56.6	0	2.31	Total
								0.39	End boxes
						15.4	0	0.83	Support posts
Date: 14-apr-'98	0.37	0	67.5	50.4	1.93	41.2	0	1.09	Net Values

Table 3.3: Results without cooling of the radiation screen

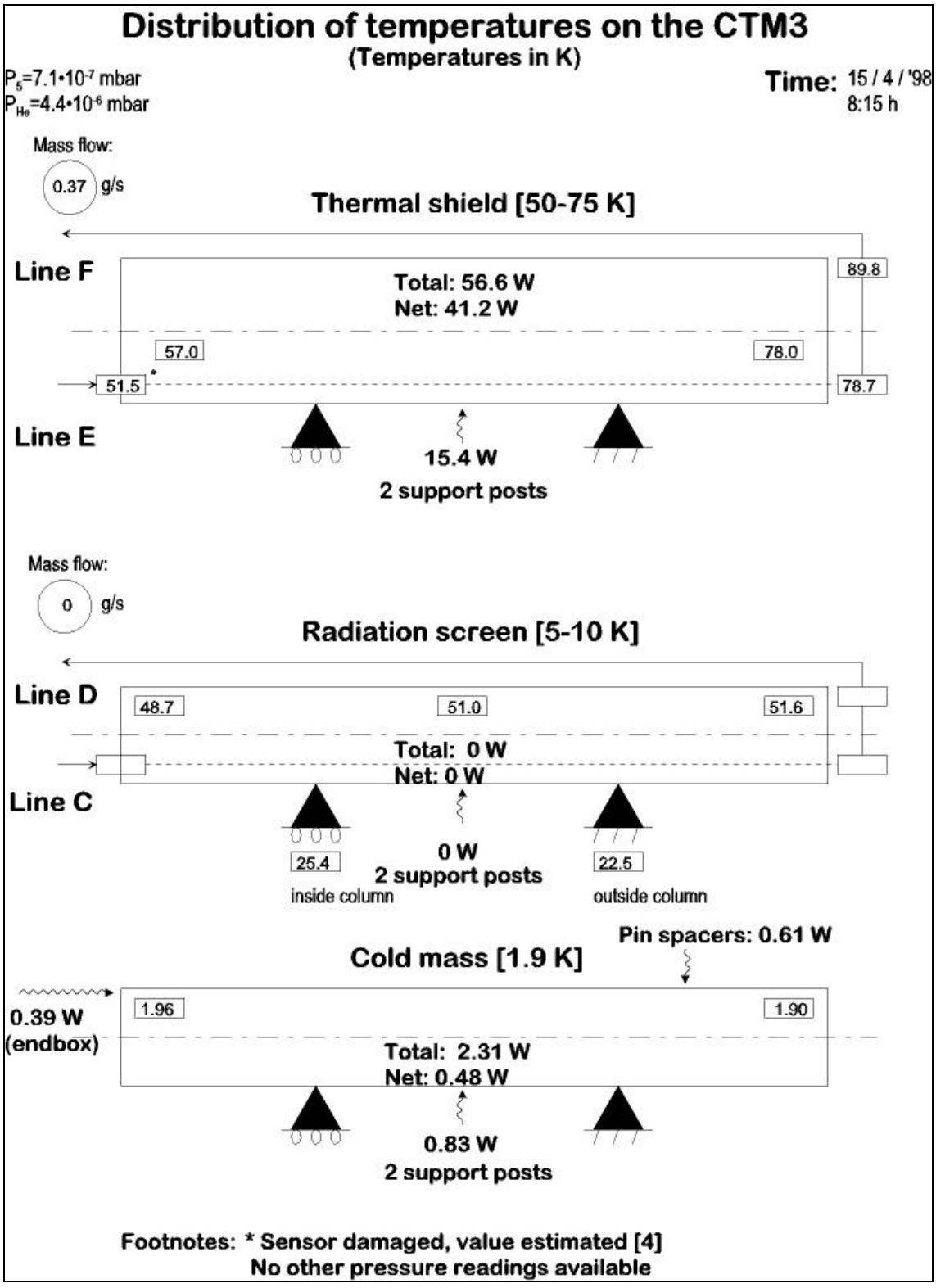

Figure 3.2: Temperature map of CTM3 for the measurement without cooling of the radiation screen

The calculated value for the support post contribution to the radiation screen is -0.08 Watts, i.e. practically zero.

Without active cooling, the equilibrium radiation screen temperature of 51 K is approximately the same as the one on the support post intercept flange.

The net value on the cold mass of approximately 1 Watt is not inconsistent with preliminary estimates of heat loads by radiation (≈ 0.3 W), conduction via the carbon spacers (≈ 0.6 W) and some conduction via the residual gas.

The results for this measurement, together with the results for the measurement series with temperature degradation of the radiation screen, are shown in Figures 3.3 and 3.4.

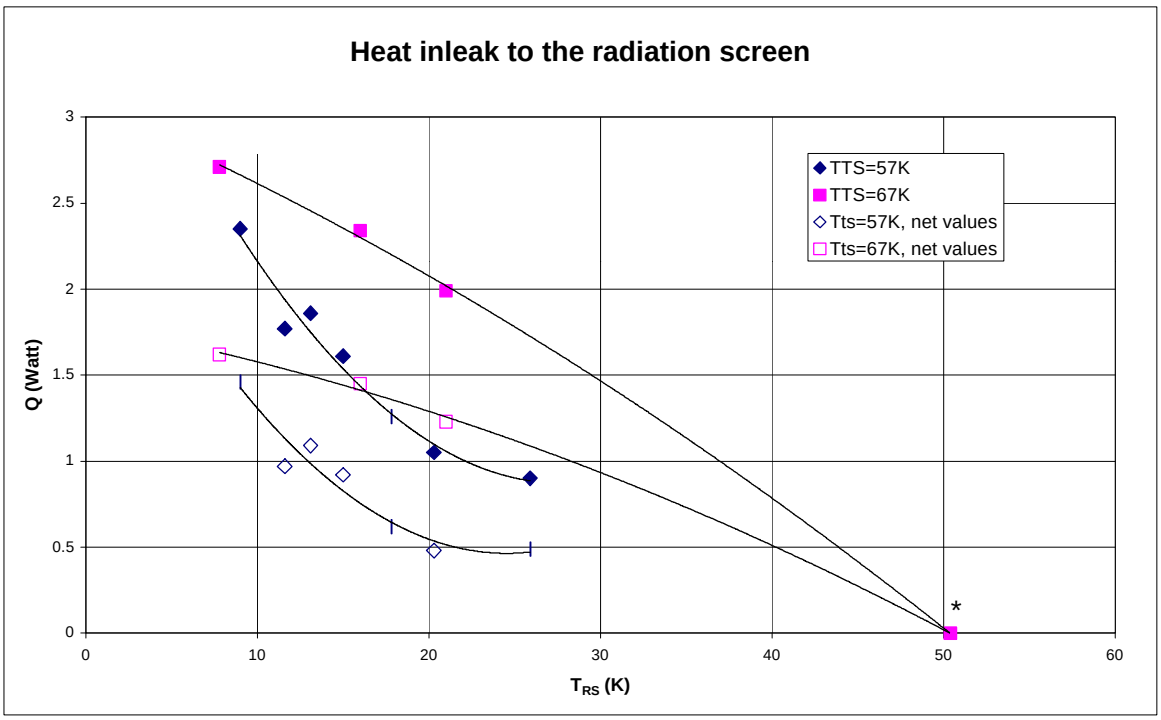

Figure 3.3: Total and net heat inleak to the radiation screen in CTM3 under degraded temperature conditions for the radiation screen, i.e. above 10 K, with a background helium pressure of $1.1 \cdot 10^{-5}$ mbar measured on the vacuum tank, and $1.6 \cdot 10^{-5}$ to $2 \cdot 10^{-5}$ mbar near the cold mass * no radiation screen cooling

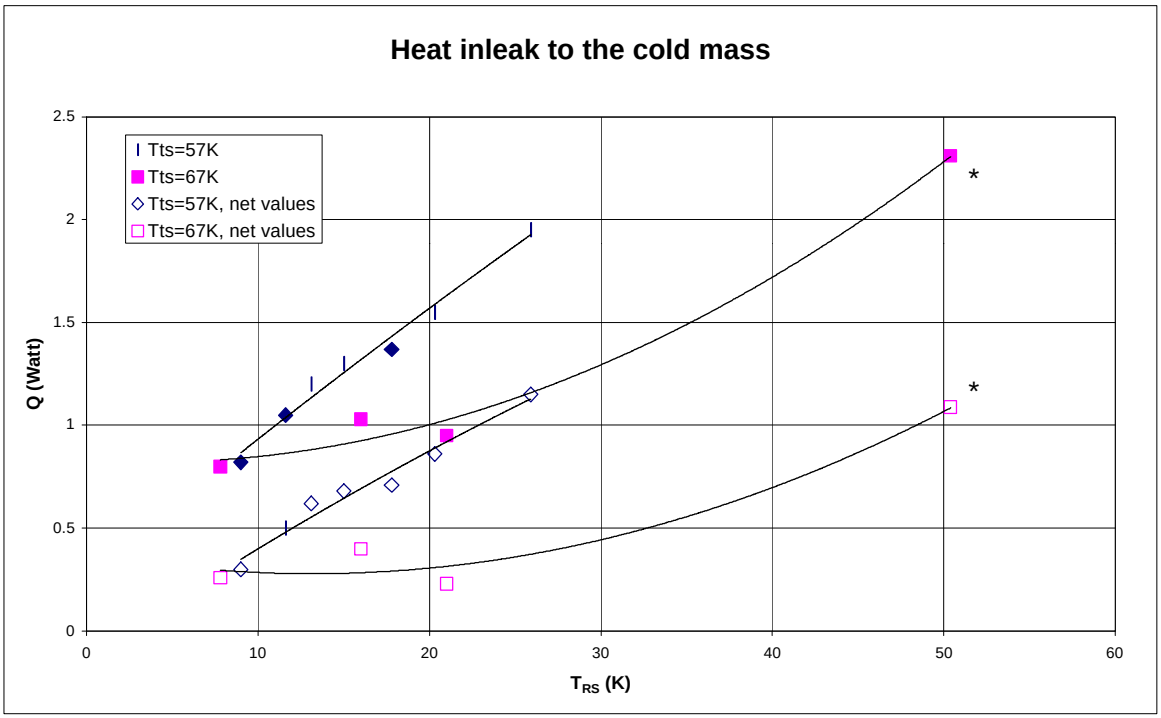

Figure 3.4: Total and net heat inleak to the cold mass under degraded temperature conditions for the radiation screen, with a background helium pressure of $1.1 \cdot 10^{-5}$ mbar measured on the vacuum tank, and $1.6 \cdot 10^{-5}$ to $2 \cdot 10^{-5}$ mbar near the cold mass * no radiation screen cooling

3.4 Measurements with insulating vacuum pressure degradation

To measure the performance of the cryostat under degraded vacuum conditions, a series of measurements was performed over a range of pressures of 10^{-3} - 10^{-4} mbar. Together with the nominal condition measurement, and the series with degraded temperature, this gives a total range of pressures from 10^{-7} to 10^{-3} mbar.

The poor vacuum conditions for reasons stated in 3.1, together with the fact that the helium-injection for the degradation of the vacuum was done manually, made it difficult to achieve steady state conditions for the measurements. The leak from the cold mass and the cryopumping on the cold surfaces and the necessity to pump the insulation vacuum with the turbo molecular pump while the helium was injected, made the regulation to arrive at a stable background vacuum pressure very difficult.

In Table 3.4, the helium gas pressures and temperatures are given and, in Table 3.5, the resulting heat loads. More details on the pressure measurements are given in Annex 1.

Helium pressures [mbar]		Temperatures [K]		
P_{warm} [293 K]	P_{cold} [≈10 K]	T_{TS}	T_{RS}	T_{CM}
$2.5 \cdot 10^{-4}$	$5.8 \cdot 10^{-4}$	68.2	12.0	8.0
$2.6 \cdot 10^{-4}$	$8.8 \cdot 10^{-3}$	68.0	11.0	6.5
$5.9 \cdot 10^{-4}$	$1.8 \cdot 10^{-4}$	69.0	9.1	5.6
$1.0 \cdot 10^{-3}$	$2.8 \cdot 10^{-3}$	71.1	18.5	11.0

Table 3.4: Temperatures and pressures in CTM3 under degraded vacuum conditions

Helium pressure	Thermal shield [W]			Radiation screen [W]			Cold mass [W]			
P_{warm} [mbar]	Total	Supp.	Net.	Total	Supp.	Net	Total	Supp.	Endb.	Net.
$2.5 \cdot 10^{-4}$	41.0	15.0	26.0	5.92	1.08	4.85	1.52	0.11	0.42	0.99
$2.6 \cdot 10^{-4}$	43.5	15.0	28.5	4.76	1.08	3.68	3.96	0.11	0.43	3.43
$5.9 \cdot 10^{-4}$	44.7	14.9	29.8	3.10	1.14	1.97	6.33	0.07	0.47	5.79
$1.0 \cdot 10^{-3}$	46.9	14.9	32.0	7.12	1.02	6.10	6.25	0.16	0.52	5.57

Table 3.5: Heat loads in CTM3 under degraded temperature conditions

The results for the total and net heat loads are also shown in Figures 3.5, 3.6 and 3.7. The results for the nominal condition and a measurement from the degraded temperature series with comparable conditions were added to these figures, to give the results for a wider range of pressures. In Figure 3.7, the total heat inleak includes the endbox contributions.

The dispersion of the measurements, resulting from unstable pressure and temperature conditions, is clearly visible in the figures. If one for instance compares the two measurements at $2.5 \cdot 10^{-4}$ mbar and $2.6 \cdot 10^{-4}$ mbar, there is a large difference in the results of these two points, even though parameters like the temperatures, mass flows and pressure are in principle comparable.

All measurements points above 10^{-4} mbar were obtained with a cold mass temperature above the λ-point, with the heat inleak measured from the enthalpy variation of the cooling gas between outlet and inlet.

The inlet and outlet temperatures of the radiation screen and the dummy cold mass are given in Figures 3.8 and 3.9.

With a limited helium mass flow rate (0.1 g/s) on the radiation screen, at these high gas densities, the radiation screen and cold mass are strongly coupled thermally by conduction through the gas. This renders extrapolation of the measured heat loads to nominal operating temperature impossible, on both the radiation screen and the cold mass.

However, the sum of radiation screen and dummy cold mass heat inleaks, shown in Figure 3.10 as a function of the background gas density, is interesting in so far as it permits thermal performance comparison with other cryostat designs without actively cooled radiation screen [10]. In this figure, the net heat load is the total heat load to radiation screen and cold mass, minus the support post contribution to the 5-10 K level.

In particular, pending further confirmation measurements, the thermal heat inleak at the low temperature stage (5-1.9 K) of this cryostat seems to be significantly lower than previous runs (CTM1 – CTM2, [7]).

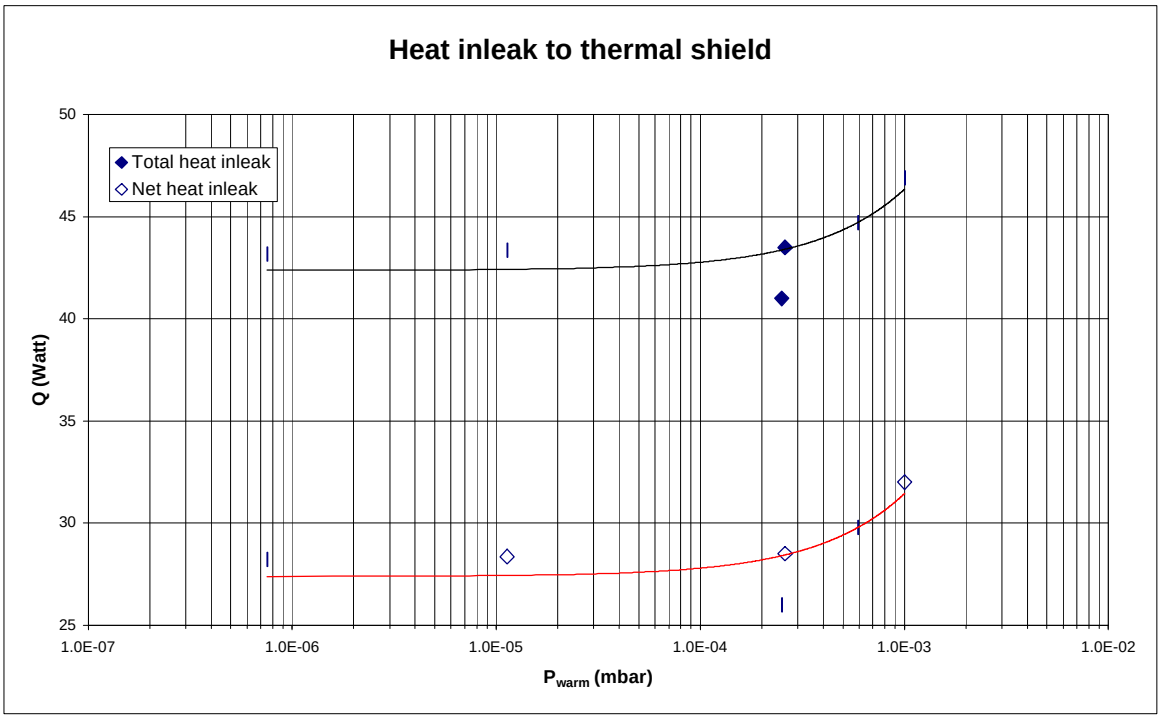

Figure 3.5: Total and net heat inleak to the thermal shield with degraded vacuum conditions. P_{warm} is the pressure measured on the vacuum vessel wall, corrected for helium

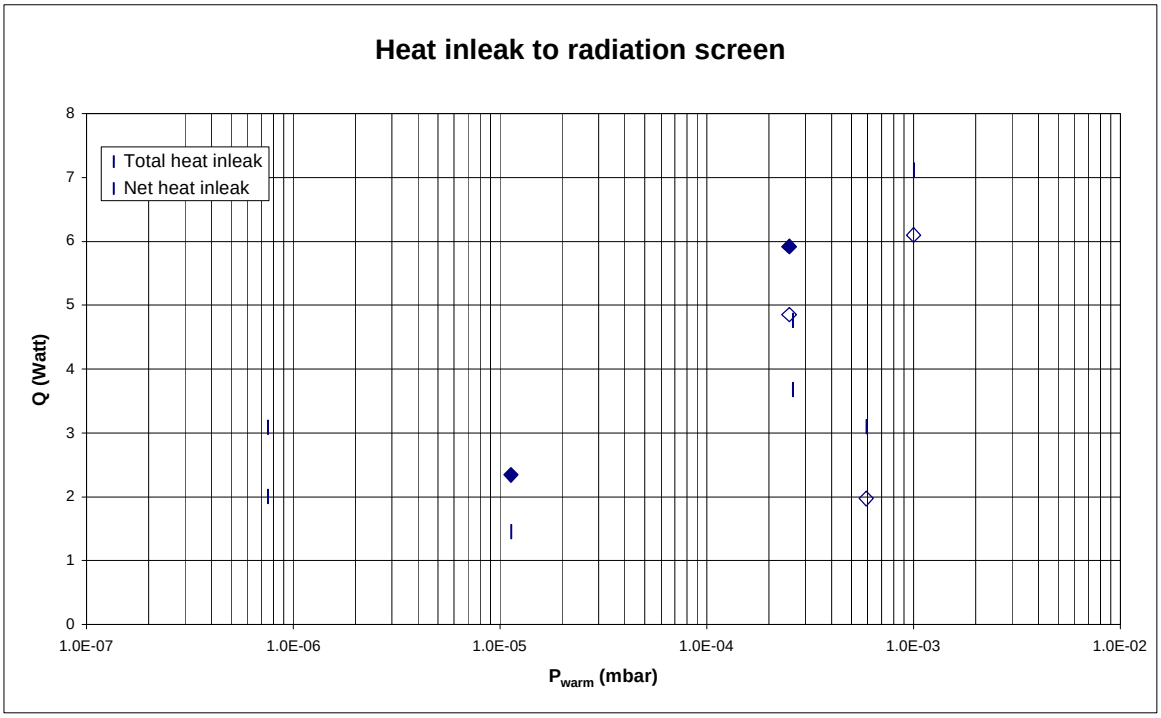

Figure 3.6: Total and net heat inleak to the radiation screen with degraded vacuum conditions. P_{warm} is the pressure measured on the vacuum vessel wall, corrected for helium

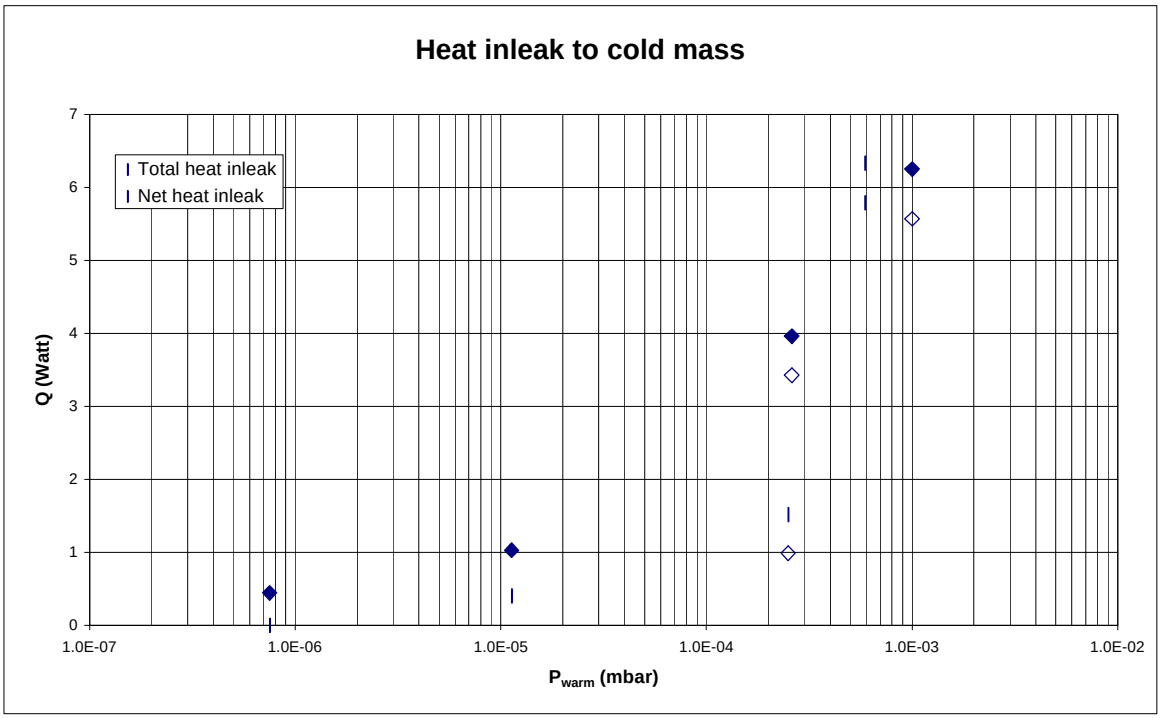

Figure 3.7: Total and net heat inleak to the dummy cold mass with degraded vacuum conditions. P_{warm} is the pressure measured on the vacuum vessel wall, corrected for helium

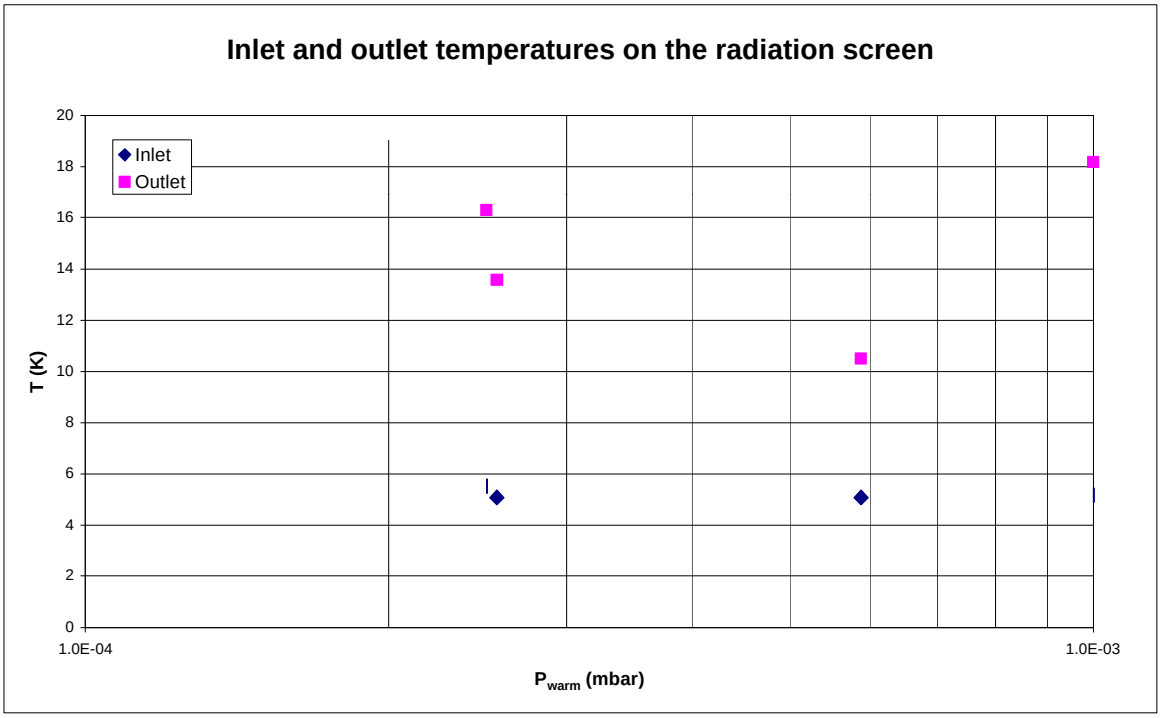

Figure 3.8: Temperatures on the radiation screen

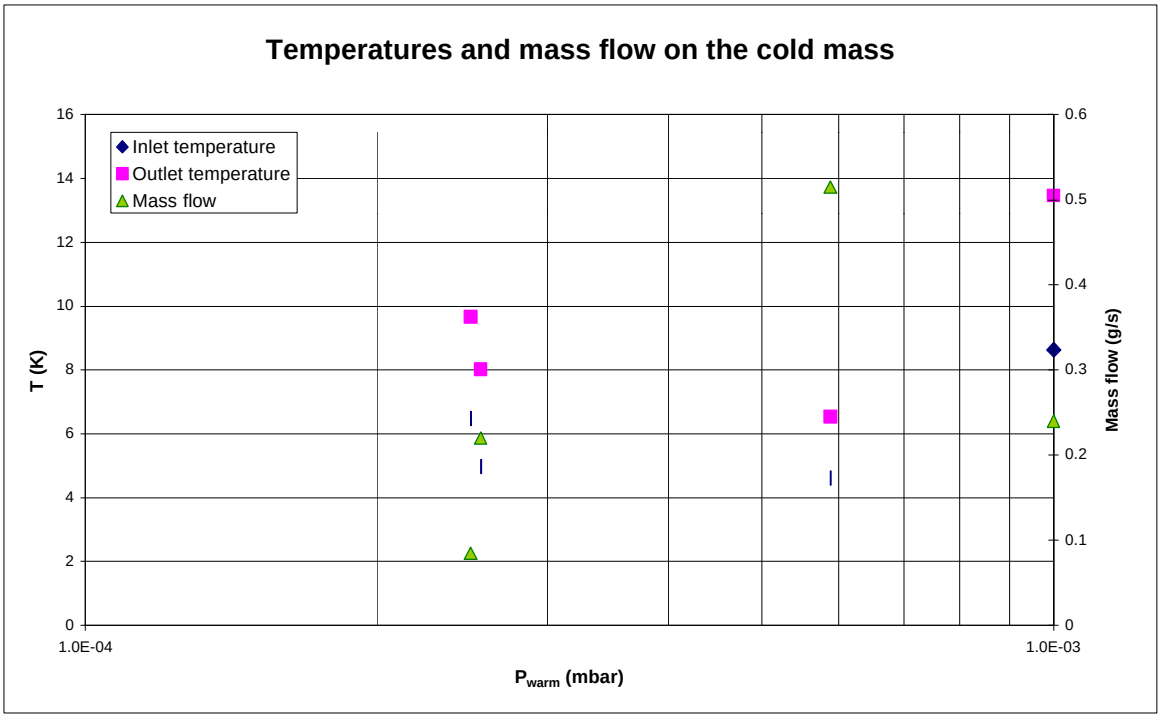

Figure 3.9: Temperatures and mass flow for the cold mass, above the λ-point. P_{warm} is the pressure measured on the vacuum vessel wall, corrected for helium

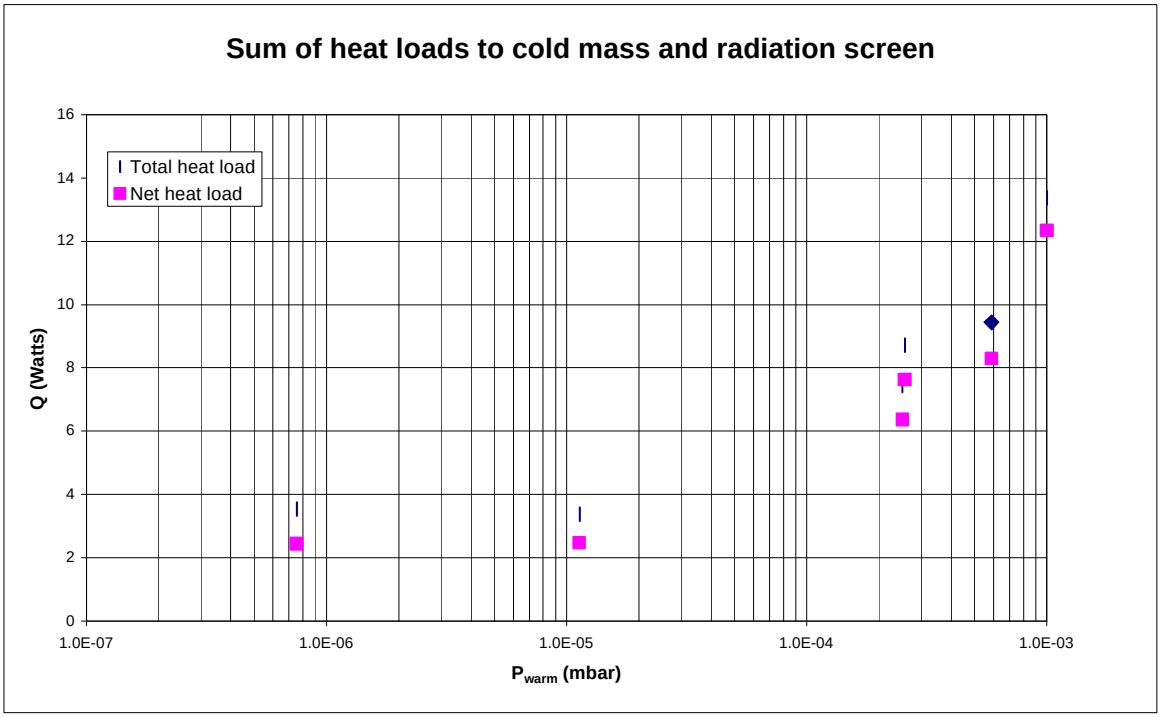

Figure 3.10: Sum of heat loads on radiation screen and cold mass. P_{warm} is the pressure measured on the vacuum vessel wall, corrected for helium

4. Preliminary conclusions and future work

As already mentioned, in CTM3 run 1 the difficulty to achieve stable conditions was the largest difficulty. Nevertheless, nominal and off-design results of the thermal performance of the CTM3 cryostat were obtained.

To improve the measurement with degraded insulating vacuum, the ongoing campaign, CTM3 - run 2, will have a repaired dummy cold mass, the availability of a quasi-constant helium supply and an automatic control of the background gas density. This should permit further validation of the performance of the CTM3 cryostat.

References

[1] C. Rabier, V. Benda: Multilayer insulation, Thesis from the mechanical engineering department of the Institut Polytechnique de Sévenans, August 1995

[2] Ch. Darve, G. Vandoni: Thermal performance of cryogenic pin spacers, LHC Project Report 220, 7 Aug. 1998

[3] Ch. Darve: Experimental programme for the CTM3, http://nicewww.cern.ch/~cdarve

[4] V. Rodillon: Utilisation d'un modèle thermique mathématique des pieds froids pour les mesures du CTM, rapport de stage de license au CERN du 1er juillet au 25 août 1998,

[5] M. Castoldi, V. Parma: Thermal Performance Calculation Model for the LHC Cold Supports, LHC-CRI-Technical Note 98-18, December 1998.

[6] M. Mathieu, V. Parma, T. Renaglia, P. Rohmig, L.R. Williams: 293 K – 1.9 K supporting systems for the Large Hadron Collider (LHC) cryo-magnets, LHC Project Report 163, 21 Jan. 1998.

[7] Ch. Darve, G. Ferlin, M. Gautier, L.R. Williams: Thermal Performance Measurements on a 10-meter long Dipole Prototype Cryostat (Cryostat Thermal Model 2), LHC Project Note 112, 11 June 1997.

[8] Balzers pressure gauge specifications

[9] Ch. Darve, Mesure des pertes thermiques nominales du modèle thermique du LHC-CRI-Technical Note 98-15, Décembre 1998.

[10] G. Riddone, Theoretical modelling and experimental investigation of the thermal performance of the LHC Prototype lattice cryostats, PhD - Thesis, Geneva, January 1997

ANNEX 1: CTM3 GAS DENSITY MEASUREMENTS

As previously said, CTM3 had Penning type gauges located on the vacuum vessel (P_5 at room temperature) inside the thermal shield (P_2 and P_4 between 70 K and 10 K) and inside the radiation screen close to the cold mass (P_1 and P_3 between 10 K and 2 K). See Figure 6.1.

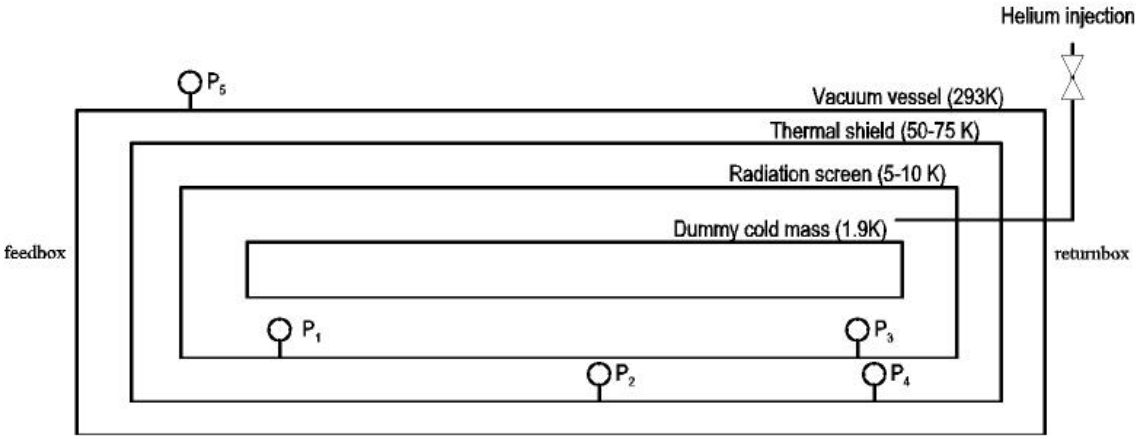

Figure 6.1: Distribution of Penning type pressure gauges on CTM3

Penning gauges calibrated in pressure for helium at room temperature (see calibration Tables 6.1 and 6.2) measure the gas density.

The behaviour of Penning gauges at low temperature is not known. Possible reasons for poor response (or false calibration) of Penning gauges at cryogenic temperatures could be:

1. Reversible magnetic field change (Penning gauges control the gas discharge with a permanent magnet, ferrite based).
2. Irreversible magnetisation change as a result of thermal cycling.
3. Conductance limitation at gauge entrance at low temperature.

The Balzers IPG100 gauges used have a low-pressure limit of 10^{-9} mbar. The discharge extinguishes below this value.

Their pumping speed is estimated to be in the range 1 – 2 l/s; their entrance conductance at 10 K is in the order of 10 l/s for helium. Therefore conductance limitation (3, above) at low temperature should not be significant.

The gauges used in CTM3 have been calibrated again after run 1. Their sensitivity has not significantly changed, indicating no irreversible effect of the thermal cycles on the magnet.

Figure 6.2 and Table 6.3 below give the reading of the gauges, for helium, during the high-pressure tests of CTM3. The pressure for the measurement done on 19/3/1998 is the same for all the points with degradation of the radiation screen temperature. The measurement done on 22/5/1998 represents the nominal condition.

It is seen that for most measurement points the pressure ratio's between different temperatures reflect more or less the thermal transpiration effect.

At equilibrium, one should have:

$$\frac{P_3(2-10K)}{P_2(70-10K)} \approx \sqrt{\frac{40}{6}} \approx 2.4 \qquad (6.1)$$

$$\frac{P_2(70-10K)}{P_5(293K)} \approx \sqrt{\frac{293}{40}} \approx 2.6 \qquad (6.2)$$

The respective measured ratio for measurement points 2 and 4 are ≈1.8 and ≈2.

The absolute difference between theoretical and experimental pressure ratios is certainly within the gauge calibration uncertainty range. However, the relative variation of the CTM3 gauge pressure readings between different measurement points as seen from figure 6.2 is certainly significative of pressure stabilisation problems of CTM3 run 1.

P_{ref} [mbar]	P_2 [mbar]	P_3 [mbar]	P_4 [mbar]
$2.8 \cdot 10^{-6}$	$3.90 \cdot 10^{-7}$	$4.30 \cdot 10^{-7}$	$4.70 \cdot 10^{-7}$
$4.77 \cdot 10^{-6}$	$6.90 \cdot 10^{-7}$	$7.30 \cdot 10^{-7}$	$8.10 \cdot 10^{-7}$
$6.00 \cdot 10^{-6}$	$9.60 \cdot 10^{-7}$	$9.80 \cdot 10^{-7}$	$1.00 \cdot 10^{-7}$
$1.30 \cdot 10^{-5}$	$1.90 \cdot 10^{-6}$	$2.00 \cdot 10^{-6}$	$2.20 \cdot 10^{-6}$
$2.44 \cdot 10^{-5}$	$4.00 \cdot 10^{-6}$	$4.00 \cdot 10^{-6}$	$4.20 \cdot 10^{-6}$
$5.2 \cdot 10^{-5}$	$1.00 \cdot 10^{-6}$	$9.80 \cdot 10^{-6}$	$9.90 \cdot 10^{-6}$
$1.2 \cdot 10^{-4}$	$2.30 \cdot 10^{-5}$	$2.10 \cdot 10^{-5}$	$2.10 \cdot 10^{-5}$
$2.06 \cdot 10^{-4}$	$4.10 \cdot 10^{-5}$	$3.80 \cdot 10^{-5}$	$3.80 \cdot 10^{-5}$
$9.50 \cdot 10^{-4}$	$1.30 \cdot 10^{-4}$	$1.10 \cdot 10^{-4}$	$1.33 \cdot 10^{-4}$
Average:	17%	16%	17%

P_{ref} [mbar]	P_1 [mbar]	P_5 [mbar]
$3.70 \cdot 10^{-5}$	$6.90 \cdot 10^{-6}$	$4.60 \cdot 10^{-6}$
$5.50 \cdot 10^{-5}$	$1.00 \cdot 10^{-5}$	$7.30 \cdot 10^{-6}$
$1.10 \cdot 10^{-4}$	$2.20 \cdot 10^{-5}$	$1.60 \cdot 10^{-5}$
$2.30 \cdot 10^{-4}$	$4.20 \cdot 10^{-5}$	$3.50 \cdot 10^{-5}$
$3.77 \cdot 10^{-4}$	$6.30 \cdot 10^{-5}$	$6.10 \cdot 10^{-5}$
$7.45 \cdot 10^{-4}$	$1.00 \cdot 10^{-4}$	$1.20 \cdot 10^{-4}$
$2.20 \cdot 10^{-3}$	$2.10 \cdot 10^{-4}$	$4.40 \cdot 10^{-4}$
Average:	16%	15%

Tables 6.1 & 6.2: Calibration of the Penning pressure gauges, at room temperature, for helium

Date	P_2 [mbar]	P_3 [mbar]	P_4 [mbar]	P_5 [mbar]
19/3/1998	$7.1 \cdot 10^{-6}$	$1.6 \cdot 10^{-5}$	$8.8 \cdot 10^{-6}$	$1.1 \cdot 10^{-5}$
6/5/1998	$1.7 \cdot 10^{-3}$	$2.8 \cdot 10^{-3}$	$2.6 \cdot 10^{-3}$	$1.0 \cdot 10^{-3}$
8/5/1998	$4.8 \cdot 10^{-4}$	$5.8 \cdot 10^{-4}$	$5.9 \cdot 10^{-4}$	$2.5 \cdot 10^{-4}$
10/5/1998	$1.0 \cdot 10^{-3}$	$1.8 \cdot 10^{-3}$	$1.4 \cdot 10^{-3}$	$5.9 \cdot 10^{-4}$
10/5/1998	$5.9 \cdot 10^{-4}$	$8.8 \cdot 10^{-4}$	$7.7 \cdot 10^{-4}$	$2.6 \cdot 10^{-4}$
12/5/1998	$8.2 \cdot 10^{-4}$	$2.9 \cdot 10^{-3}$	$7.7 \cdot 10^{-4}$	$4.3 \cdot 10^{-4}$
22/5/1998			$2.7 \cdot 10^{-8}$	$7.5 \cdot 10^{-7}$

Table 6.3: Pressures in CTM3

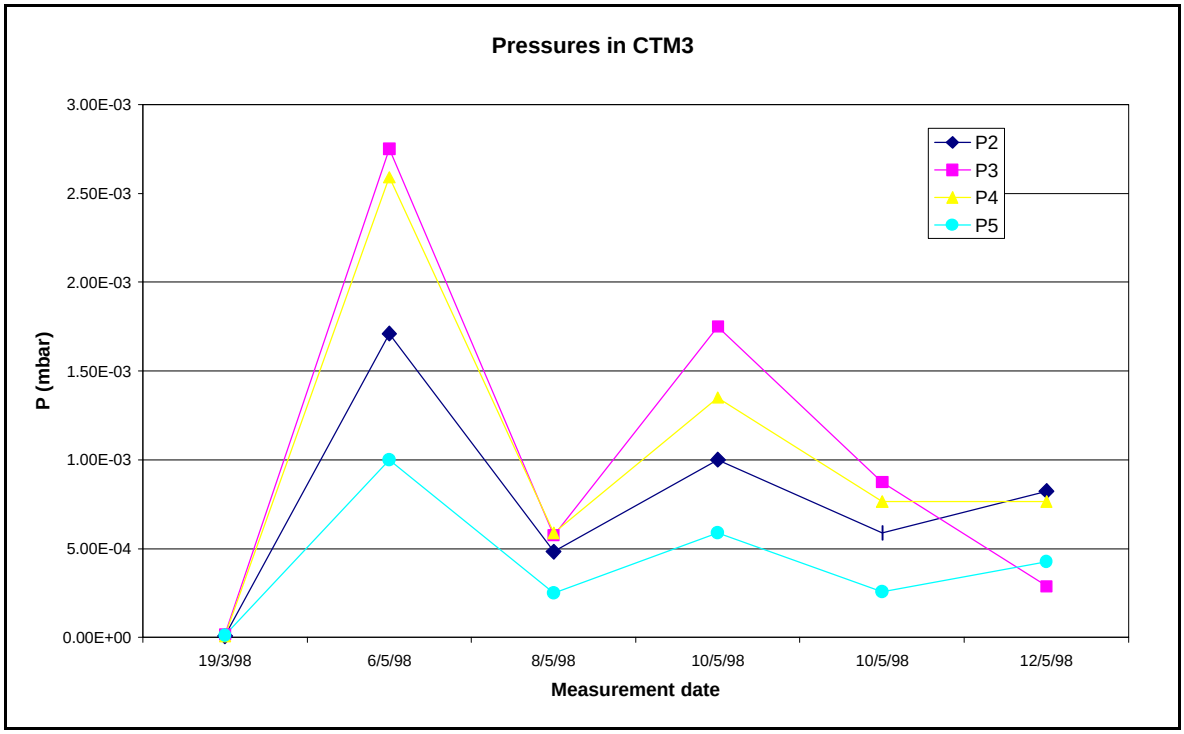

Figure 6.2: Pressures in CTM3

LHC-CRI Technical Note 98-19

Distribution:

Bozzini D.	LHC-CRI
Brunet J-C.	LHC-CRI
Buenaventura A.	LHC-CRI
Burla P.	LHC-CRI
Clerc R.	TIS-TE
Cruikshank P.	LHC-VAC
Darve Ch.	LHC-CRI
Dauvergne J-P.	LHC-ECR
Erdt W.	LHC-ACR
Evans L.	DG-DI
Faugeras P.	AC-DI
Gourber J-P.	AC-DI
Gröbner O.	LHC-VAC
Hauviller Cl	EP-TA1
Jacquemod A.	LHC-CRI
Jenninger B.	LHC-VAC
Kershaw K.	EST-ESI
Kowalczyk P.	LHC-CRI
Lebrun Ph.	LHC
Nielsen L.	LHC-CRI
Parma V.	LHC-CRI
Poncet A.	LHC-CRI
Proudlock P.	AC-TCP
Quesnel J-P.	EST-SU
Renaglia Th.	EST-ESM
Riddone G.	LHC-ACR
Rieubland J-M.	LHC-ECR
Rohmig P.	LHC-CRI
Rousselin A.	LHC-CRI
Sacré Ph.	LHC-CRI
Savary F.	LHC-MMS
Scandale W.	LHC-MMS
Skoczen B.	LHC-CRI
Siegel N.	LHC-ICP
Sievers P.	LHC-MTA
Struik M.	LHC-CRI
Taylor T.	LHC
Tavian L.	LHC-ACR
Vandoni G.	LHC-ECR
Vlogaert J.	LHC-MMS
Wikberg T.	EST-LEA
Willems D.	LHC-CRI
Williams L.R.	LHC-CRI
Wyss C.	LHC-MMS